PCCP

PAPER

View Article Online
View Journal | View Issue

Cite this: *Phys. Chem. Chem. Phys.*, 2015, **17**, 31125

Interplay between solid state transitions, conductivity mechanisms, and electrical relaxations in a [PVBTMA] [Br]-*b*-PMB diblock copolymer membrane for electrochemical applications†

Vito Di Noto,*[a] Guinevere A. Giffin,[b] Keti Vezzù,[a] Graeme Nawn,[a] Federico Bertasi,[a] Tsung-han Tsai,[c] Ashley M. Maes,[d] Soenke Seifert,[e] E. Bryan Coughlin[c] and Andrew M. Herring*[d]

Received 16th September 2015,
Accepted 16th October 2015

DOI: 10.1039/c5cp05545h

www.rsc.org/pccp

Understanding the structure–property relationships and the phenomena responsible for ion conduction is one of the keys in the design of novel ionomers with improved properties. In this report, the morphology and the mechanism of ion exchange in a model anion exchange membrane (AEM), poly(vinyl benzyl trimethyl ammonium bromide)-*block*-poly(methylbutylene) ([PVBTMA][Br]-*b*-PMB), is investigated with small angle X-ray scattering, high-resolution thermogravimetry, modulated differential scanning calorimetry, dynamic mechanical analysis, and broadband electrical spectroscopy. The hyper-morphology of the material consists of hydrophilic domains characterized by stacked sides of [PVBTMA][Br] which are sandwiched between "spaghetti-like" hydrophobic cylindrical parallel domains of the PMB block. The most important interactions in the hydrophilic domains occur between the dipoles of ammonium bromide ion pairs in the side chains of adjacent chains. A reordering of the ion pair dipoles is responsible for a disorder–order transition (T_δ) at high temperature, observed here for the first time in AEMs, which results in a dramatic decrease of the ionic conductivity. The overall mechanism of long range charge transfer, deduced from a congruent picture of all of the results, involves two distinct ion conduction pathways. In these pathways, hydration and the motion of the ionic side groups are crucial to the conductivity of the AEM. Unlike the typical perfluorinated sulfonated proton-conducting polymer, the segmental motion of the backbone is negligible.

Introduction

In the last decade the field of anion exchange membranes (AEMs) has seen a resurgence of interest since the suggestion that they could serve as the separator in a polymer electrolyte fuel cell.[1] We are now in a situation where a large number of AEM materials have been synthesized and proposed for a number of diverse applications.[2] AEMs are anion conducting materials suitable for the development of separation and filtration applications,[3] alkaline polymer electrolyte fuel cells[1,4] alkaline polymer electrolyte electrolysers,[5] redox flow batteries,[6] reverse electrodialysis cells,[7] and bioelectrochemical systems including microbial fuel cells[8] and enzymatic fuel cells.[9] Anion exchange membrane fuel cells (AEMFCs) are a family of devices able to harness the chemical energy obtained by the electro-oxidation of fuels such as hydrogen or small organic molecules (*e.g.*, alcohols), and convert it directly into electrical energy with a high efficiency.[10,11] AEMFCs utilize an anion-exchange membrane (AEM) able to transport the OH^- anions produced at the cathode of the cell to the anode, where they undergo recombination with the products of the fuel oxidation.[4] The AEM gives rise to a strongly alkaline environment at the electrodes; thus, AEMFCs may adopt oxygen reduction electrocatalysts which do not include rare elements such as the platinum-group metals (PGMs), dramatically reducing device costs and the likelihood of electrode supply bottlenecks.[12] Finally, AEMs efficiently block fuel

[a] *Department of Industrial Engineering, Section of Chemistry for Technology and Energy & Department of Chemical Sciences, University of Padova, Via Marzolo 1, I-35131 Padova, Italy. E-mail: vito.dinoto@unipd.it*
[b] *Helmholtz Institute Ulm (HIU), Electrochemistry I, Helmholtzstrasse 11, 89081 Ulm, Germany & Karlsruhe Institute of Technology (KIT), P. O. Box 3640, 76021 Karlsruhe, Germany*
[c] *Department of Polymer Science and Engineering, University of Massachusetts Amherst, 120 Governors Drive, Amherst, MA 01003, USA*
[d] *Department of Chemical and Biological Engineering, Colorado School of Mines, Golden, CO 80401, USA. E-mail: aherring@mines.edu*
[e] *X-Ray Sciences, Advanced Photon Source, Argonne National Laboratory, Argonne, Illinois 60439, USA*
† Electronic supplementary information (ESI) available. See DOI: 10.1039/c5cp05545h

crossover; consequently, they can be very thin, giving rise to devices characterized by a very high power density.[13]

When applied to electrochemical devices such as redox flow batteries, reverse electrodialysis cells and microbial fuel cells the migrating anion can be F^-, Cl^-, Br^-, I^- *etc.* On the basis of the anion equivalent conductivity in water solutions at room temperature,[14] the conductivity of the AEMs decreases in the order of increasing anion size $F^- > Cl^- > Br^- > I^-$.[15] Crucial to this is the host polymer structure and its nano-structured morphology in modulating the chemical, thermal, electrochemical stability, and the conductivity of AEM membranes. AEMs are based on a backbone chain, which provides the thermomechanical stability to the membranes and different side chains, containing cationic groups to enable anionic conductivity.[4] The cationic groups mostly consist of ammonium-, sulfonium- or phosphonium-based functional groups.[2,16] The polymer backbone can be a polyether polysulfone,[17–19] poly(arylene ether),[20,21] poly(phenylene),[22,23] poly(phenylene oxide),[24–27] polystyrene,[28–32] poly(ethylene),[33–35] poly(isoprene)[36] or poly(ether-imide).[37,38] The main properties explored for each of the proposed AEMs are their ion-exchange capacity (IEC), water uptake (W.U.), chemical and thermal stability, and conductivity at different hydration states.[16]

A drawback of the OH^- form of AEMs, hydroxide exchange membranes (HEMs), is carbonation upon exposure to 400 ppm of CO_2 present in the atmosphere, or the products of the oxidation of hydrocarbon fuels.[39] Carbonation significantly alters the thermomechanical and electrical properties of the membranes. In contrast, the physical properties of the anion exchange membranes in the halide-form (X exchange membranes, XEMs, where X = halide), such as BrEM and ClEM, are not affected by the presence of CO_2. XEMs, with respect to the parent HEMs, are more thermally and chemically stable films that can be manipulated in the open air and allow a more facile study of important film properties.[16,40] There is also an advantage that simple trimethylbenzylammonium cations, which are not necessarily stable to attack by the nucleophilic hydroxide at elevated temperatures or under dry conditions, can be used in these model systems.

The common strategy to improve the ionic conductivity of an AEM is to increase its IEC. A high IEC significantly influences the mechanical properties in a negative manner, leading to dramatic fragility and brittleness when the membrane is completely dry and can lead to excessive swelling when the material is wet, making the material unusable for practical applications.[16] In order to overcome the drawbacks described above, the design and synthesis of new membranes need to be addressed by a consolidated understanding of the interplay that exists between the structure, properties, relaxation phenomena, and long range anion migration mechanisms in AEMs. Unfortunately, few studies are found in the literature that elucidate the correlations between anion transport phenomena, physical properties, and the cooperative dynamics of the polar side group and polymer backbone relaxations of AEMs. To date much effort in understanding the properties of AEMs has been dedicated to studies of the interaction and dynamics of solvated anions in bulk membranes and the effect of water uptake on these dynamics.[15,16,41–43] The correlation between host polymer dynamics and the conductivity mechanism was recently investigated in detail for the Selemion AMV® membrane which consists of two components: a functionalized polystyrene copolymer containing the ammonium ion-exchange moieties and poly(vinyl chloride).[44] The Selemion AMV® was studied both in the Cl^- and OH^- forms. Two predominant pathways of charge exchange through the membrane were found to contribute to the overall conductivity of the material. One, through the bulk of the hydrophilic domains that is associated with the electrode polarization and the other, along the interface between the hydrophobic and hydrophilic domains associated with the inter-domain polarization. This pioneering study, for the first time, highlights the significant difference existing between anion and proton exchange membranes in terms of the contribution of the dynamics of the polymer backbone matrix to the long range charge migration processes. Indeed, it was demonstrated that, in the Selmion AMV® membrane there is significant contribution of the backbone matrix dynamics to the anion migration processes which are strongly modulated by the polymer nano-structured morphology. Results from this AEM show that the conduction process is correlated with the dynamics of the host backbone matrix, in contrast with those of PEMs which are highly dissociated ionic systems.[45–47]

The detailed investigation of AEMs in their halide form is a crucial stepping-stone to improve the fundamental understanding of how the physicochemical features of the membranes, with a particular reference to the micro-structures, thermomechanical properties, the electric response, and the influence of hydration, are correlated with the long range charge transfer mechanism. In this report, the aim is: (a) to investigate the structural relaxations governing the thermo-mechanical and electrical events in the poly(vinyl-benzyl-trimethyl-ammonium-bromide)-*b*-poly(methyl-butylene) ([PVBTMA][Br]-*b*-PMB) membrane; and (b) to study the mechanism of conduction. The analysis of the correlations existing between electrical relaxations and structural and thermo-mechanical properties is of crucial importance for the elucidation of the strategic parameters and phenomena which will influence future syntheses to improve the performance of next generation AEMs for application in practical devices.

In detail in this paper, the micro-structure is studied by small angle X-ray scattering (SAXS), the thermal stability and transitions are detected by high-resolution thermogravimetry (HR-TG) and by modulated differential scanning calorimetry (MDSC), respectively. The mechanical properties and transitions are investigated by dynamic mechanical analysis (DMA). Broadband electrical spectroscopy (BES) is used to study the electric response and the conductivity mechanisms of the membranes in the frequency and temperature range of $0.01–10^7$ Hz and $-105–100$ °C, respectively. BES is a powerful technique, which allows us to fully understand the overall electric response and dielectric relaxations of the membranes, both in a completely dry state and after full hydration, thus allowing the clarification of the role played by both ion solvation phenomena and the water cluster structure in the performance of these materials. The integration of the information acquired from all of these

techniques allows us to propose a reasonable mechanism for the long range charge migration processes in [PVBTMA][Br]-*b*-PMB.

Experimental methods

Reagents and materials

A poly(vinylbenzyltrimethylammonium bromide)-*b*-poly(methylbutylene) ([PVBTMA][Br]-*b*-PMB) block polymer was synthesized at the University of Massachusetts Amherst as reported elsewhere.[48] The [PVBTMA][Br]-*b*-PMB membrane with a bromide exchange capacity of 2.2 mEq g^{-1} was used as received. The dry membranes were prepared by drying the material for 48 h under vacuum at room temperature. The dry membranes were kept under an argon atmosphere inside a dry-box and transferred and handled in an argon atmosphere. The full hydrated samples (wet) consist of [PVBTMA][Br]-*b*-PMB immersed in an argon atmosphere in double-distilled water. Solvents were supplied by Aldrich and further purified by standard methods. Bi-distilled/milli-Q water was used in all procedures.

Instruments and methods

Thermogravimetric analyses were performed with a high resolution TGA 2950 (TA Instruments) thermobalance using a working N_2 flux of 100 mL min^{-1}. The TG profiles were collected in the temperature range between 25 and 800 °C with a heating rate varied from 40 to 0.001 °C min^{-1} depending on the first derivative of the weight loss. Approximately 5 mg of the material was analyzed in an open platinum pan. The water uptake was determined by TGA measurements as described elsewhere[49] after soaking the samples in water at room temperature for two days. The initial (wt_0) and dry (wt_{dry}) weight of each sample was determined by registering the isothermal TGA desorption profile at 30 °C. The W.U. was determined using the following equation:

$$\text{W.U.} = \frac{\text{wt}_0 - \text{wt}_{\text{dry}}}{\text{wt}_{\text{dry}}} \times 100$$

MDSC measurements were carried out in the cyclic mode (two cycles) using a MDSC 2920 differential scanning calorimeter (TA Instruments) equipped with a LNCA low-temperature attachment operating under a helium flux of 30 cm^3 min^{-1}. Measurements are performed at a heating rate of 3 °C min^{-1} between −150 and 100 °C on about 4 mg of the sample in a hermitically-sealed aluminum pan.

Dynamic mechanical analyses (DMA) are carried out with a TA Instruments DMA Q800 instrument, using the film/fiber tension clamp. The temperature spectra, in the range from −100 to 100 °C at a rate of 4 °C min^{-1}, are measured by subjecting a rectangular dry film sample (*ca.* 25 mm (height) × 6 mm (width) × 0.05 mm (thickness)) to an oscillatory sinusoidal tensile deformation at 1 Hz with an amplitude of 4mm, and with a 0.02 N preload force.

BES spectra were collected in the frequency range from 0.01 to 10^7 Hz and the temperature range from −105 to 150 °C using a Novocontrol Alpha-A analyzer. The temperature was increased in 10 °C increments using a home-made cryostat operating with a N_2 gas jet heating and cooling system. The temperature was measured with an accuracy higher than ±0.4 °C. The geometrical cell constant was determined by measuring the electrode–electrolyte contact surface and the distance between the electrodes. No corrections for the thermal expansion of the cell were used. The complex impedance ($Z^*(\omega) = Z'(\omega) + iZ''(\omega)$) was converted into complex conductivity ($\sigma^*(\omega) = \sigma'(\omega) + i\sigma''(\omega)$) and complex permittivity ($\varepsilon^*(\omega) = \varepsilon'(\omega) - i\varepsilon''(\omega)$) using the equations $\sigma^*(\omega) = k[Z^*(\omega)]^{-1}$ and $\sigma^*(\omega) = i\omega\varepsilon_0\varepsilon^*(\omega)$, respectively, where k is the cell constant in cm^{-1} and $\omega = 2\pi f$ (f is the frequency in Hz). The wet sample was soaked in water for two hours prior to measurement and 100 μL of double-distilled water was added to the measurement cell. For all techniques unless otherwise specified, the membrane was dried under vacuum for two days prior to measurement.

SAXS data were obtained using beamline 12IDC-D at the Advanced Photon Source (APS) at Argonne National Laboratory, Argonne, IL using X-rays of 18 keV. The samples were mounted in an environmental chamber described previously,[50] at a temperature of 60 °C. The wet sample was soaked in DI water for 24 h, blotted dry and immediately placed in the environmental chamber at 95% RH.

DFT calculations

The dipole moment of vinyl-benzyl-trimethyl-ammonium-bromide repeat units was calculated after geometry optimization using density functional theory methods on the basis of an all-electron DFT code using the DMol3 program[51,52] as a part of the Material Studio package.

The double numerical plus polarization basis set and gradient-corrected (GCA) BLYP functional was adopted. *N*,*N*,*N*-trimethyl-(4-ethylphenyl)methanaminium bromide was used as fragment to evaluate the ion-pair dipole moment (ip-μ) of charged polar repeat units.

Results and discussion

Composition, water uptake, morphology and thermal stability

The [PVBTMA][Br]-*b*-PMB AEM consists of a block copolymer whose structure is shown in Scheme 1. A and B are the hydrophilic and hydrophobic blocks, respectively.

The A block consists of a statistical distribution of n = 250 repeat units based on both vinylbenzyltrimethylammonium bromide ([VBTMA][Br]) and 4-methylstyrene (4MS). The percentage of [VBTMA][Br] is DF% = $n_{[\text{VBTMA}][\text{Br}]}/(n_{[\text{VBTMA}][\text{Br}]} - n_{[4\text{MS}]})\cdot 100$ = 89.4% where $n_{[\text{VBTMA}][\text{Br}]}$ and $n_{[4\text{MS}]}$ are the moles of [VBTMA][Br] and 4MS repeat units, respectively. The B block consists of m = 590 repeat units of methylbutylene. It is expected that the larger hydrophobic B block modulates the structural features and chemically, mechanically, and thermally stabilizes the ionomer.

The [PVBTMA][Br]-*b*-PMB membrane has a high water uptake from liquid water (*ca.* 125%) and exhibits significant through-plane swelling. The through-plane swelling percentage

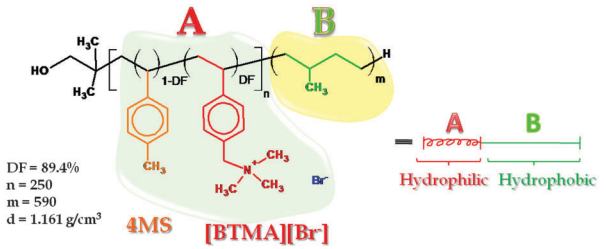

Scheme 1 Structure of the [PVBTMA][Br]-*b*-PMB block copolymer. A is the hydrophilic domain and B is the hydrophobic domain.

is *ca.* 200%, and the in-plane swelling is *ca.* 15%, thus illustrating considerable anisotropy that can be explained by the morphology of the membrane.

The polymer has an IEC of 2.2 mmol g^{-1} and the lambda value of the fully swollen AEM is 31. Lambda refers to the hydration number which corresponds to the number of water molecules per ammonium group. This is in stark contrast to the random lightly cross-linked polymer of similar composition and an IEC of 2.34 mmol g^{-1} where the water uptake is 515% and λ = 122.[36]

The dry and wet SAXS of the film are shown in Fig. 1 and are similar to the SAXS for a similar material with slightly lower IEC.[53] The anomalous SAXS tuned to the energy of Br was identical to the SAXS (not shown) indicating that the scattering of these materials is dominated by the Br containing, hydrophilic regions of the polymer. A peak at low Q is followed by a series of reflections indicating long range lamella morphology of the hydrophilic phase for both dry and wet samples as seen in some compositions of the lamella phases of the sulfonated analogue polystyrenesulfonate-*b*-polymethylbutylene (PSS-*b*-PMB).[54] For the dry material the *d*-spacing (from $Q = 2\pi/d$) was 49 nm and the q*, 2q*, 3q* were observed. The wet film has a *d* spacing of 97 nm and the q*, 2q*, 3q*and 5q* peaks are observed more strongly as the long range order is increased. 4q* for the wet film is not seen due to destructive interference. We propose that the hyper-morphology of the material (inset of Fig. 1) consists of ''spaghetti-like'' hydrophobic cylindrical parallel domains consisting of B blocks of PMB chains which are sandwiching the hydrophilic A domains that along the PVB backbone chains are characterized by a statistical distribution of a mixture of stacked side chains of both [PVBTMA][Br] and the 4MS repeat units.

Given that only the structural difference between PSS-*b*-PMB[54] and [PVBTMA][Br]-*b*-PMB is in the ionic group, it is reasonable to assume that the overall morphology would be similar and consistent with the structural hypothesis shown in the inset of Fig. 1. As water is absorbed into the polar domains of the PSS or the [PVBTMA][Br] matrix, the membrane would swell perpendicular to the direction of the hydrophobic PMB domains (the *z* direction of the inset of Fig. 1). This scenario explains the very large through-plane swelling and the comparatively small in-plane swelling and the water uptake and λ values of [PVBTMA][Br]-*b*-PMB AEM.

The HR-TG profiles of the [PVBTMA][Br]-*b*-PMB membrane, both in the dry and in the wet state, are shown in Fig. 2. The TG

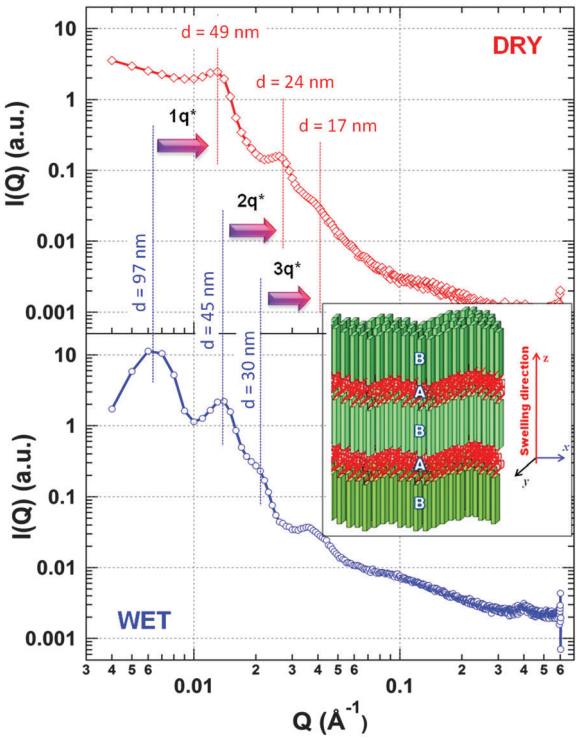

Fig. 1 SAXS patterns of [PVBTMA][Br]-*b*-PMB membranes recast from THF at 60 °C under dry conditions and of the soaked film at 95% RH. The hydrophobic B domains are in green while hydrophilic A domains are shown schematically in red (B > A). *x*, *y* and *z* swelling directions of the membrane are indicated where $x \approx y \ll z$.

profile shows a small mass loss that starts at 100 °C and continues until about 150 °C. This mass loss, which constitutes about 2.5% of the total mass, is likely due to traces of water. [PVBTMA][Br]-*b*-PMB undergoes a significant elimination at *ca.* 230 °C, event I, which is associated with the loss of the ammonium group from the PVBTMA block ($-TMA^+Br^-$). This evidence is in accordance with results described elsewhere,[55] which illustrate that poly[(*p*-vinylbenzyl) dimethyl-2-hydroxyalkyl ammonium chloride] polyelectrolytes exhibit a mass elimination at 200 °C while polystyrene and chloromethylated polystyrene are thermally stable up to *ca.* 350 °C. The thermal phenomenon II is ascribed to the degradation of the PMB block and it is detected at $T \sim 410$ °C, which shows that this block has a significant thermal stability. This assignment is in accordance with studies on isotactic poly(3-methyl-1-butene) which demonstrated that this polymer undergoes less than a 5 wt% mass loss up to *ca.* 400 °C.[56] The comparison of dry and hydrated HR-TGA profiles shows that the initial hydration state of the [PVBTMA][Br]-*b*-PMB membrane does not significantly affect the thermal stability of the membrane when the bulk absorbed water is removed at low temperatures (Fig. 2). Nevertheless, the I and II thermal events of the fully hydrated sample are shifted to higher temperatures by *ca.* 10–15 °C as compared to the dry [PVBTMA][Br]-*b*-PMB membrane. The slight inhibition of the thermal degradation demonstrates that the residual water molecules form a polar solvation shell for the $-TMA^+$ cation which acts to stabilize the polar groups in bulk materials.

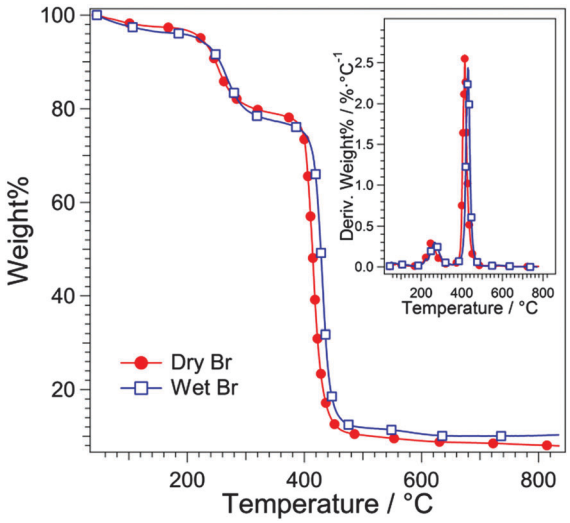

Fig. 2 HR-TG profiles of the [PVBTMA][Br]-*b*-PMB membrane, both in the dry and at the full hydration state. The inset shows the derivative of HR-TG profiles. The curve of the fully hydrated sample is normalized to the wt% at T = 45 °C.

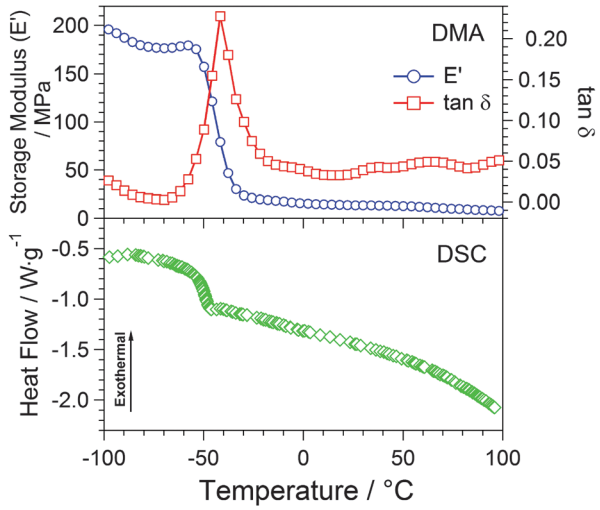

Fig. 3 DMA (top) and DSC (bottom) profiles of dry [PVBTMA][Br]-*b*-PMB. The storage modulus (E') at 1 Hz is shown on the left axis and tan δ is shown on the right axis.

Thermo-mechanical transitions

The thermal and mechanical properties and transitions of the [PVBTMA][Br]-*b*-PMB AEM in the dry state are studied by DMA and MDSC from −100 up to 100 °C.

The DSC, DMA storage modulus and the DMA tan δ curves of [PVBTMA][Br]-*b*-PMB are shown in Fig. 3.

The DSC profile shows only a glass transition (T_g) at −51 °C in the explored temperature range (Fig. 3). This T_g is significantly lower than that of either of the polymer blocks based on data for their respective homopolymers. Poly(3-methyl-1-butene) (PMB) and poly(4-methylstyrene) (P4MS) have T_g at 50 and 100 °C, respectively.[57] Therefore, the alkyl ammonium functionalities and the structure of the diblock polymer backbone chains modulate the morphology (shape and size of hydrophobic and hydrophilic domains), which significantly reduces T_g, which is largely associated with the segmental motion of PMB blocks.

The mechanical properties and transitions of the material are closely linked to T_g. The storage modulus undergoes a step-decrease from 183 MPa before to 20 MPa at the glass transition temperature, while tan δ exhibits a peak at T_g. After the glass transition the storage modulus of the material is quite constant with increasing temperature. This mechanical behavior is very different from that of dry Nafion®. The storage modulus of dry Nafion® shows a slow decrease until about 100 °C where it abruptly drops.[58] This drop is due to a reduction of the electrostatic interactions within Nafion®'s polar domains.[58] This difference in behavior is due to the nature of Nafion®'s polar domains which is expected to be very different from those in [PVBTMA][Br]-*b*-PMB. The mechanical properties of dry [PVBTMA][Br]-*b*-PMB are mostly maintained by the steric hindrance phenomena between the [VBTMA][Br] side groups of the polar A domains which are promoted by the inter-chain electrostatic dipole–dipole interactions occurring due to the presence of side groups with dipole moments with opposite directions (Fig. 4). The ion pair dipole moment (ip-μ) of the [VBTMA][Br] side group is ip-μ = 11.45 D as calculated by DFT methods.

Ip-μ is generated when neighboring contact [quaternary alkyl ammonium]-[bromide] ion couples (Fig. 4) are present in the side chains of the hydrophilic A domains. Therefore, the transitions detected by both the DMA and DSC measurements are the results of two independent but coupled phenomena which take place when the thermal motions of the backbone and side chains increase up to a limiting temperature value where a concurring weakening occurs of: (a) the inter-chain ion pair dipole–dipole interactions of the side chains; and (b) the van der Walls interactions of the PMB backbone chains. As such, the thermal T_g transition is coupled to the DMA relaxation event because the decrease of the inter-side-chain interactions,

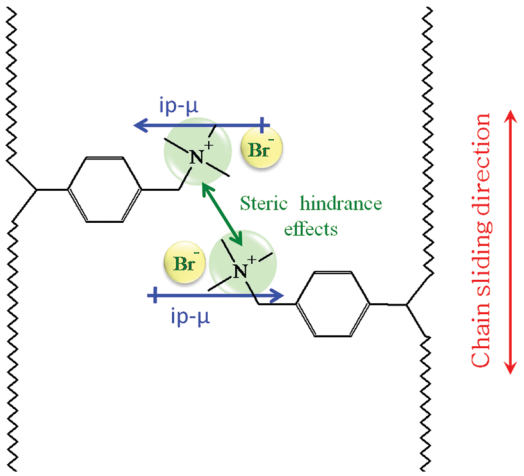

Fig. 4 Steric effects governed by inter-chains electrostatic dipole–dipole interactions between ion-pair dipole moments (ip-μ) of [PVBTMA][Br] functionalities.

and therefore steric hindrance phenomena, results in an improved sliding ability of the polymer backbone chains to slide reciprocally, thus reducing the elastic modulus of the material.

This scenario is different from that of dry Nafion® where mesoscale interactions between hydrophobic and hydrophilic domains are mostly correlated with hydrogen bonding interactions between un-dissociated sulfonic acid moieties in the hydrophilic domains. In this case, the influence of steric phenomena on thermal and mechanical properties is expected to be negligible.

Electric relaxations and the conductivity mechanism

The parameters used to quantify the electric response are determined by fitting the real and imaginary components of the permittivity and conductivity profiles of the BES measurements by a suitable model over a range of temperatures and frequencies. These parameters are crucial to elucidate the mechanism of conduction within the material especially when combined with results determined with techniques such as SAXS, DSC, and DMA.

The three-dimensional ε', ε'' and $\tan\delta$ surfaces and contour plots of dry [PVBTMA][Br]-*b*-PMB are shown in Fig. 5a–d, respectively.

It should be observed that while the measurements were conducted up to 155 °C, the spectra are only shown up to 115 °C. Above 115 °C a sharp drop in the permittivity values is seen which corresponds to a disorder–order solid-state transition. This event, which occurs in the hydrophilic domains of the material and is assigned as T_δ, is discussed in more detail below. For the sake of clarity Scheme 2 depicts the assigned molecular relaxation modes, which are responsible for the host polymer dynamics in the dry [PVBTMA][Br]-*b*-PMB membrane that we describe below. The assignments are confirmed later in the text from the results of the modeling of the BES data.

The $\tan\delta$ surface represented as a contour plot (Fig. 5d) is particularly useful in identifying the electric events that are present in [PVBTMA][Br]-*b*-PMB. $\tan\delta$ shows six peaks that move from lower to higher frequencies with increasing temperature (see Fig. 5c and d). The two weakest peaks are an α event that is present in the high frequency side of the intense peak at medium frequencies and a very weak relaxation β_{PMB} which is found at the highest frequencies and lowest temperatures. These events are also visible as peaks in the ε'' surface (Fig. 5b) and three of them are clearly seen as inflection points in the ε' surface (Fig. 5a). The two lowest frequency events, which have ε' values between 10^2 and 10^6, are associated with polarization phenomena. The lower frequency polarization, σ_{EP}, is assigned to the electrode polarization phenomenon, which is caused by the accumulation of charge at the membrane-electrode interface due to the use of blocking measurement electrodes.[59]

The higher frequency polarization, σ_{IP}, is associated with an interdomain polarization phenomenon (IP). IPs are the result

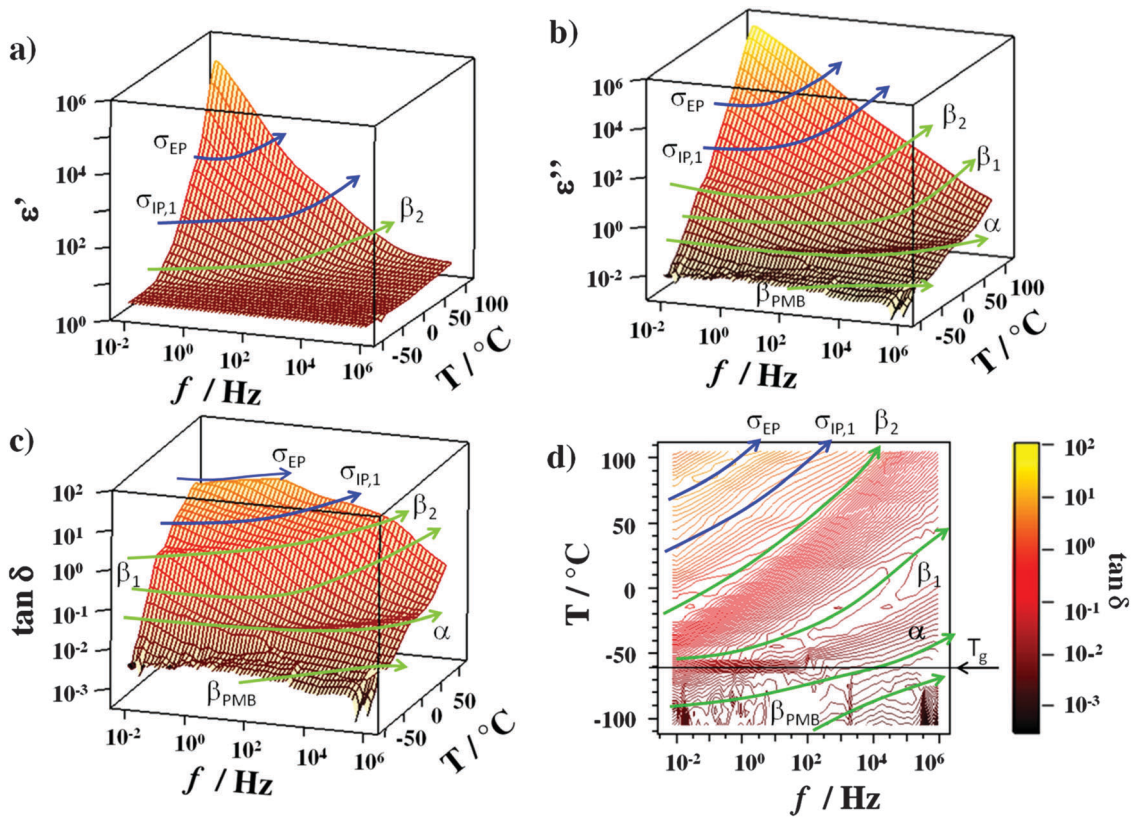

Fig. 5 Three-dimensional ε' (a), ε'' (b) and $\tan\delta$ surfaces (c) and contour (d) plots of dry [PVBTMA][Br]-*b*-PMB membranes. The blue lines refer to the polarization phenomena and the green to the dielectric relaxations. T_g is shown in (d).

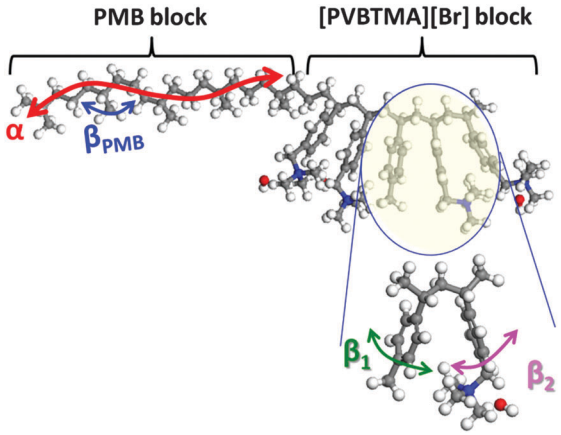

Scheme 2 Molecular dielectric relaxations of the [PVBTMA][Br]-*b*-PMB membrane. The α-mode corresponds to the diffusion of conformational states along PMB backbone chains (segmental motions) in B domains; the β_{PMB}-mode is the local fluctuation of the dipole moment of MB repeat units; β_1- and β_2-modes are the fluctuations of the local dipole moments of the tolyl and benzyl trimethyl ammonium side groups, respectively, in hydrophobic A domains.

of the accumulation of charge at the interfaces between nanodomains in the bulk membranes characterized by different permittivities.[59]

In the [PVBTMA][Br]-*b*-PMB membrane, the IP is associated with charge accumulated at the interface between the polar domains based on [PVBTMA][Br] blocks and the nonpolar domains due to the aggregation of the PMB block polymer fragments. The four high frequency events seen in Fig. 5, which have permittivity values less than 10^2, are assigned to molecular relaxation phenomena. The two highest frequency relaxations (α and β_{PMB}) are associated with the PMB blocks. The higher frequency event, β_{PMB}, is associated with the local fluctuation of the dipole moment of the methylbutylene repeat units, while the lower frequency event, α, is assigned to the segmental motion of the PMB blocks. Similar relaxations have been previously assigned in polybut-1-ene.[60] The other two molecular relaxations, β_1 and β_2, occur with slower dynamics and are associated with the local fluctuations of the dipole vectors of the tolyl (4MS) and functionalized quaternary ammonium side groups ([VBTMA][Br]), respectively, of the hydrophilic A blocks. It should be noted that the α-relaxation associated with the segmental motion of the [PVBTMA][Br] blocks cannot be discerned at lower frequencies from the experimental spectrum as it is likely covered by the much higher permittivity values of the polarization phenomena.

The three-dimensional ε', ε'' and $\tan\delta$ surfaces and the contour map of the wet [PVBTMA][Br]-*b*-PMB are shown in Fig. 6. The permittivity values seen in Fig. 6 are as much as four orders of magnitude larger than those in the dry membrane in Fig. 5. Five relaxation events can be discerned in the $\tan\delta$ surface of the wet membrane (Fig. 6c and d). However, the phenomenological origin of some of these events is different than in the dry

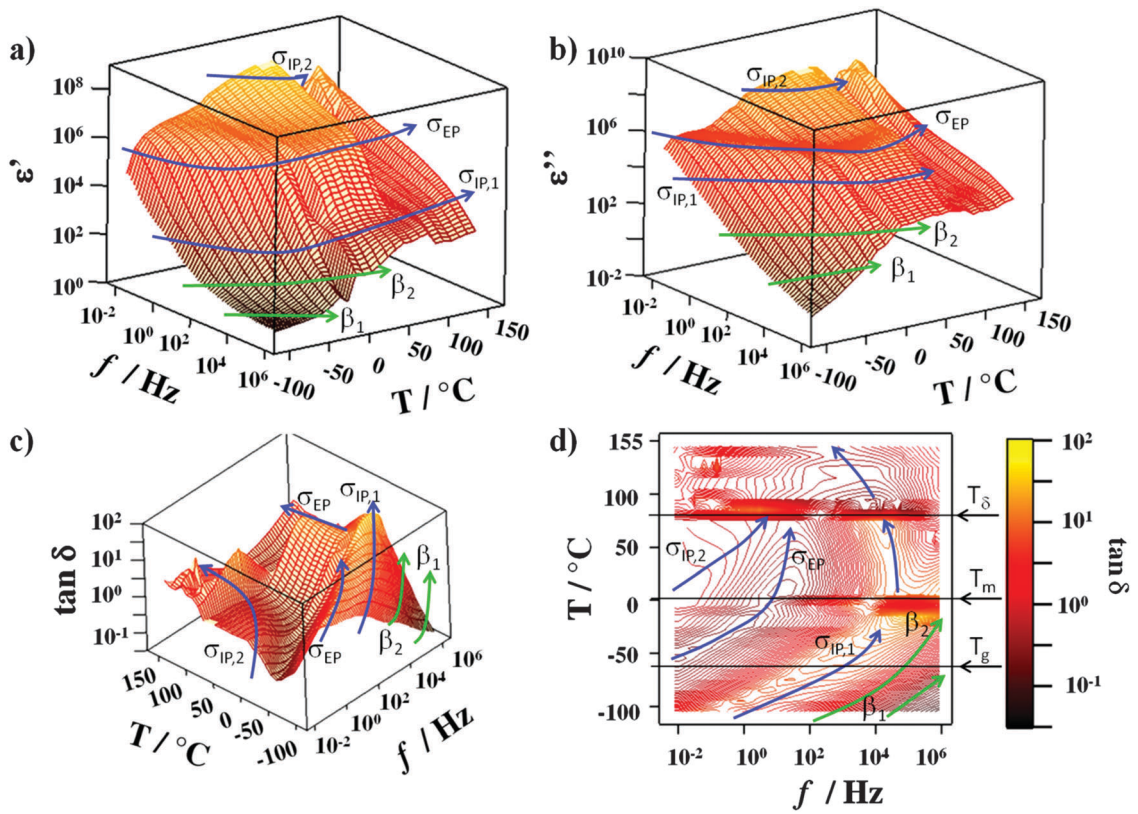

Fig. 6 Three-dimensional ε' (a), ε'' (b) and $\tan\delta$ surfaces (c) and contour (d) plots of wet [PVBTMA][Br]-*b*-PMB membranes. Thermal transitions T_g, T_m and T_δ are shown in (d).

membrane. The two highest frequency relaxations are assigned to the β-relaxations of the tolyl and benzyl trimethyl ammonium side groups in the A hydrophilic [PVBTMA][Br] blocks, β_1 and β_2, respectively. The three lower frequency relaxations are associated with polarization phenomena $\sigma_{IP,1}$, σ_{EP} and $\sigma_{IP,2}$ (Fig. 6a–d). The lowest frequency polarization, $\sigma_{IP,2}$, has a much lower intensity in tan δ and occurs with much slower dynamics. A comparison with the electric response of the dry membrane allows us to assign two types of IP, $\sigma_{IP,2}$, and $\sigma_{IP,1}$ to the wet AEM.

There are two other points that can be seen from the examination of these 3D surfaces. The first comes from the observation that a significant drop in the permittivity occurs at medium and low frequencies above 85 °C in the wet membrane which corresponds to the T_δ transition previously mentioned for the dry membrane. In this temperature region the electrical response is dominated by the polarization phenomena. Therefore, a reduction in the permittivity in this region of the spectrum is related to a decrease in the conductivity (Fig. 7a and b) which is likely prompted by a disorder–order transition.

This event triggers a structural rearrangement of the –TMA$^+$Br$^-$ side groups of different chains having oriented opposite directions (see Scheme 3) and results in an ordering of the ion pair dipole moments. After T_δ, the interaction of these ion pairs results in a significant reduction of the density of charge carriers (Br^- anions) free to move in the A domains. The T_δ event in the dry membrane was observed at a slightly higher temperature (*ca.* 115 °C).

The decrease of the T_δ temperature in the wet membrane is explained if we consider that in the hydrophilic domains water molecules act to form solvation shells around –TMA$^+$Br$^-$ polar

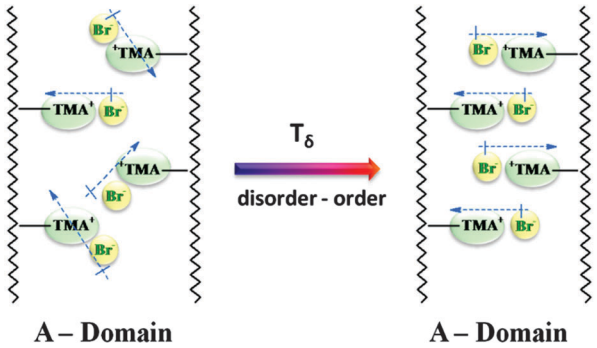

Scheme 3 Disorder–order transition, T_δ, in A hydrophilic domains. At T_δ the randomly oriented ion-pair local dipole moments (ip-μ) of R-TMA$^+$Br$^-$ side groups are ordered together coupling the ip-μ's of different backbone chains.

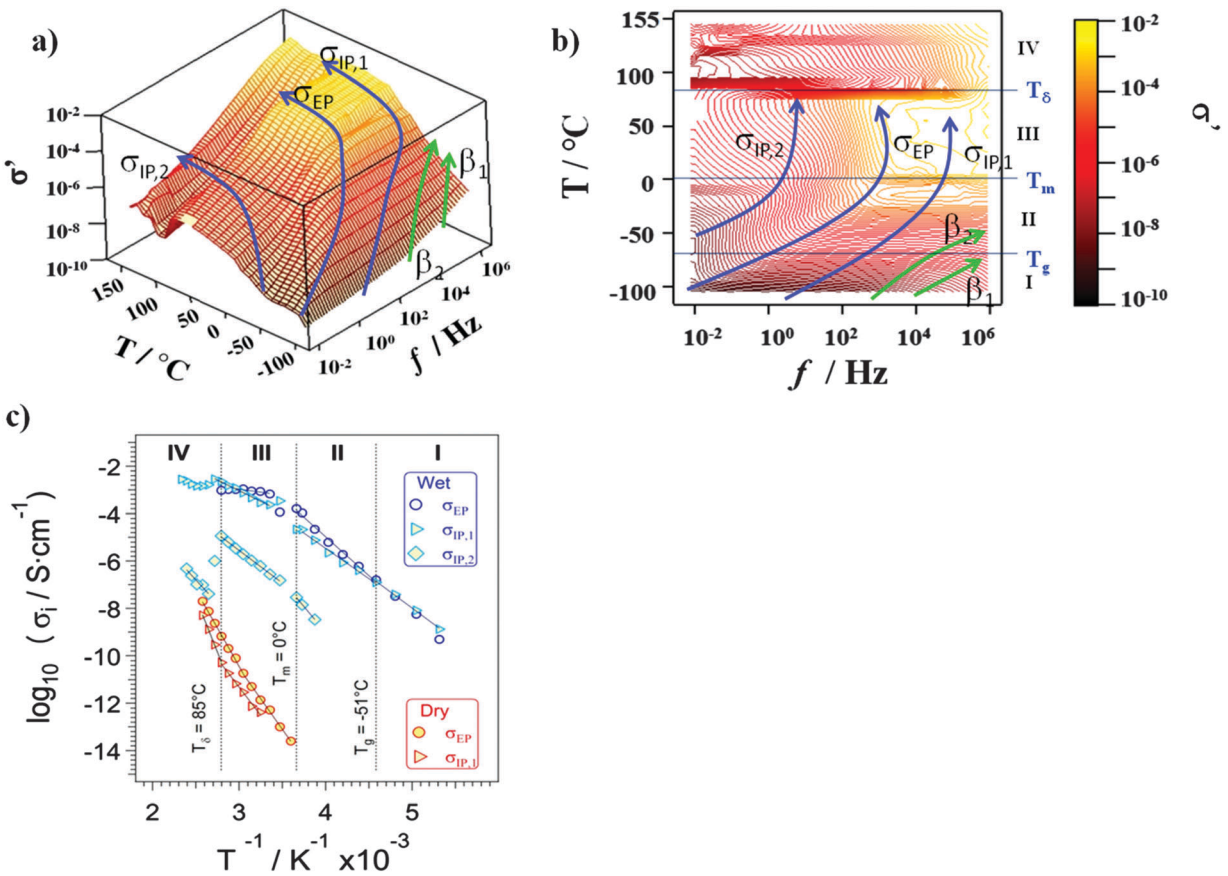

Fig. 7 Three-dimensional surface (a) and the contour plot (b) of $\sigma'(\omega)$ profiles of wet [PVBTMA][Br]-*b*-PMB membranes. Dependence of conductivity σ_i ($\sigma_i = \sigma_{EP}$, $\sigma_{IP,1}$ and $\sigma_{IP,2}$) on the inverse of temperature (1/*T*) (c). σ_i values are determined by fitting simultaneously the profiles of $\sigma^*(\omega)$, $\varepsilon^*(\omega)$ and tan $\delta(\omega)$ with eqn (1). σ_i *vs.* 1/*T* curves of dry and wet samples in I, II, III and IV regions, delimited by thermal transitions T_g, T_m and T_δ, are fitted by Arrhenius-like behaviours (c).

side groups plasticizing the hydrophilic domains and facilitating the reciprocal movements of the polar side chains.

A second important result is that there is only a small increase in the permittivity associated with the melting of water (T_m). This is very different from what is observed for Nafion® and the 3M PFSA membrane where a large step increase of several orders of magnitude occurs at 0 °C[45,59,61] and corresponds to a change in the conductivity mechanism from an Arrhenius to a Vogel–Tammann–Fulcher (VTF) form due to the very mobile chains in PFSAs.[61] The lack of such an increase in [PVBTMA][Br]-*b*-PMB would suggest that the change of state of water embedded in the membrane does not lead to a significant modification of its properties and mechanism of conduction, because the polymer is more rigid. No molecular relaxations associated with PMB blocks are visible in the wet membrane.

The most important parameters describing the overall electric response of the wet materials are: the conductivity values, associated with the polarization events; the dielectric strengths; and the characteristic relaxation times of molecular relaxation modes.

A careful determination of all the parameters is obtained by fitting simultaneously all the experimental profiles of $\varepsilon'(\omega)$, $\sigma'(\omega)$ and $\tan\delta(\omega)$, with the model described by eqn 1:[59]

$$\varepsilon^*(\omega) = -i\left(\frac{\sigma_0}{\omega\varepsilon_0}\right) + \sum_{j=1}^{3}\frac{\sigma_j(i\omega\tau_j)^{\gamma_j}}{i\omega\left[1+(i\omega\tau_j)^{\gamma_j}\right]} + \sum_{k=1}^{4}\frac{\Delta\varepsilon_k}{\left[1+(i\omega\tau_k)^{\nu_k}\right]} \quad (1)$$

The first term describes the residual conductivity that occurs at frequencies significantly lower than that can be experimentally measured (σ_0 is the background conductivity at very low frequencies and ε_0 is the permittivity of the vacuum). The second term describes the polarization phenomena. The third term represents the molecular relaxations through a Cole–Cole type equation[59] and the fourth term, ε_∞, is the electronic contribution to the permittivity of the material. The variables σ_j and τ_j are the conductivity and relaxation time associated with the *j*th event, while γ_j is a shape parameter that describes the broadness and asymmetry of the *j*-th peak. The variable *k* corresponds to the events β_{PMB}, α, β_1 or β_2. $\omega = 2\pi f$ is the angular frequency of the electric field, τ_k is the relaxation time of the *k*-th event of intensity $\Delta\varepsilon_k$, and ν_k is the shape parameter bound to the distribution of the relaxation times associated with the *k*-th event.

The 3D-$\sigma'(\omega)$ surfaces (Fig. 7a) demonstrate that the electric response of the wet membrane is mostly dominated by the polarization phenomena described above. The $\sigma'(\omega)$ contour plot (Fig. 7b) and the values of $\log\sigma_i$ ($\sigma_i = \sigma_{EP}$, $\sigma_{IP,1}$ and $\sigma_{IP,2}$), reported as a function of reciprocal temperature in Fig. 7c, show four conductivity regions (I, II, III and IV) which are delimited by the thermal transitions described above: T_g, the melting point of water, T_m, and the order–disorder transition, T_δ.

There is a difference of 6 to 12 orders of magnitude between the wet and dry conductivities of [PVBTMA][Br]-*b*-PMB. In this material, water acts to solvate the ionic ammonium bromide ion pairs reducing the electrostatic interactions between ip-μ of different side chains and increasing the mobility, both of the anion and of the –TMA$^+$ polar side chains (the plasticizing effect of water). The dry conductivity $\sigma_{IP,1}$ increases from 2.5×10^{-14} at 5 °C to 2.0×10^{-8} at 115 °C and shows a very strong thermal dependence (see Fig. 7c). In general in polymers, the conductivity associated with the electrode polarization (σ_{EP}) characterizes the "bulk conductivity" (σ_T) of the material.[58,61–63] However, in dry [PVBTMA][Br]-*b*-PMB the interdomain polarization $\sigma_{IP,1}$ is within one order of magnitude of the conductivity associated with the electrode polarization (Fig. 7c) σ_{EP}, and as a result provides an important contribution to the overall conductivity ($\sigma_T = \sigma_{EP} + \sigma_{IP,1}$). Both $\sigma_{IP,1}$ and σ_{EP} follow Arrhenius behavior characterized by very high E_a (see following discussion) in all conductivity regions (Fig. 7c). Arrhenius behavior indicates that in the dry membrane the conduction proceeds *via* percolation migration pathways where the mobile species, *i.e.* the bromide ion, moves from one coordination site to the next *via* exchange processes followed by local relaxations and structural reorganizations of the entire surrounding host matrix.

As shown in Fig. 7c wet [PVBTMA][Br]-*b*-PMB is characterized by three conductivities, $\sigma_{IP,1}$, σ_{EP}, and $\sigma_{IP,2}$. All three conductivities exhibit Arrhenius behavior both above (III and IV) and below the melting point of water (I and II). This indicates that in all temperature regions, as in the dry [PVBTMA][Br]-*b*-PMB membrane, the conduction pathway is basically correlated with anion exchange processes between different interaction sites through elementary hopping events. As was noted above, this is different from the behavior that is exhibited by Nafion®, where the melting of the water is associated with a change in behavior from an Arrhenius to a VTF form.[61] This evidence suggests that in the [PVBTMA][Br]-*b*-PMB membrane the matrix is very rigid and the dynamics of the hydrophobic backbone matrix (B domain) is not significantly correlated with the long range charge migration processes.

Over the entire temperature range, the values $\sigma_{IP,1}$ and σ_{EP} have the same order of magnitude but different relaxation time. This phenomenon reveals that there are two different pathways of conduction through the A polar domains that follow different physical mechanisms with different relaxation frequencies.

In the lowest temperature region, I, the values of log $\sigma_{IP,1}$ and log σ_{EP} can be fit by a single Arrhenius equation. The material's glass transition marks the temperature between region I and II. From the glass transition to the melting point of water (II → III), σ_{EP} is larger than $\sigma_{IP,1}$ but has a higher E_a as indicated by the slopes of the curves. Above the melting point of water, the two conductivities converge, at which point $\sigma_{IP,1}$ becomes larger than σ_{EP}. The conductivity σ_{EP} is relatively constant in region III suggesting that it follows a percolation pathway that is not highly dependent on temperature. In region IV, there is a single pathway for conduction and the overall conductivity decreases at $T > T_\delta$.

As previously shown (Scheme 3) at T_δ the conductivity is reduced due to the decrease of the density of the "free to move" Br^- anions. This event occurs when a disorder–order reorganization phenomenon in the A domains takes place by means of strong electrostatic interchain interactions between

ip-μ's which localize the Br^- anions. The conductivity σ_{EP} cannot be detected above T_δ, which suggests that the σ_{EP} conductivity pathway is more closely associated with the anion dissociation process coupled with the local disorder of the ammonium polar side groups than $\sigma_{IP,1}$. By considering the behavior of $\sigma_{IP,1}$ and σ_{EP} in all four temperature regimes, it can be hypothesized that σ_{EP} is associated with a percolation pathway through the bulk A polar domains, while $\sigma_{IP,1}$ involves a percolation pathway along the interface between the bulk A polar domains and the vinylbenzyl ammonium groups. The higher E_a above the glass transition and the relatively constant conductivity in region III support this hypothesis. The interface would be more affected compared to the bulk of the polar domain by the glass transition that provides more mobility to the polymer chains and results in a higher E_a. However, the interface is less affected by the melting of water compared to the bulk polar domain, which causes the increase seen in the conductivity of σ_{EP}.

The conductivity $\sigma_{IP,2}$ is associated with an IP phenomenon. The dynamics of this conduction process is slower and is characterized by a higher E_a than either $\sigma_{IP,1}$ or σ_{EP}. $\sigma_{IP,2}$ likely follows a percolation pathway along the A/B interface of the polar A domains and the hydrophobic PMB B domains. The presence of at least one IP in both the wet and dry membrane supports the interpretation that the [PVBTMA][Br]-*b*-PMB membrane has the lamella phase separated morphology we described and reflecting that, seen also in the TEM results[54] of the lamella PSS-*b*-PMB system, there is a good separation between the hydrophilic substituted polystyrene domains and the hydrophobic PMB domains.

The dependence of the relaxation frequencies and dielectric strengths of the molecular relaxation events on reciprocal temperature is shown in Fig. 8a and b, respectively. These results allow us to confirm the assignments of the molecular relaxations made in Scheme 2. In the dry [PVBTMA][Br]-*b*-PMB membrane, four molecular relaxations are detected. The β_{PMB} and the α relaxations are characterized by the lowest dielectric strength (Fig. 8b) and the highest frequencies (Fig. 8a). Both of these relaxation events are associated with the PMB blocks in the hydrophobic B domains. The β_{PMB} is associated with the local dipole fluctuations of the methylbutylene repeat units. The dielectric strength of α only slightly increases with temperature (Fig. 8b). The values of log f_α (Fig. 8a) follow a VTF dependence[63] up to about 35 °C (regions II and III) with a pseudo-activation energy of 11 ± 1 kJ mol^{-1}. The VTF dependence, which indicates that the relaxation mode is associated with the dynamics of the main polymer chain,[63] supports the assignment of α to the segmental motion of the PMB main polymer chains. The pseudo-E_a associated with α is about an order of magnitude smaller than the E_a of the conductivity (see Fig. 9). This disparity suggests that the segmental motion of the PMB blocks of the B domains has little impact on the overall conductivity. The two lower frequency molecular relaxations in the dry membrane, as previously discussed (Scheme 2), are associated with the fluctuations of the dipole vectors of the benzyl (β_1) and quaternary ammonium moieties in the side groups of the hydrophilic A domains (ip-μ of β_2). These are the only two relaxations that are detected in the wet membrane. Under both conditions, the β_1 and β_2 relaxations follow Arrhenius behaviour as is normal for the dipole fluctuations of the side groups[59] (Fig. 8a). The β_1 relaxation has a higher characteristic frequency and a significantly smaller dielectric ($\Delta\varepsilon$) strength than the β_2 relaxation (Fig. 8a and b). In the theory of Debye improved for polymers by Onsager, Froelich and Kirkwood,[64] $\Delta\varepsilon$ is proportional to the square of relaxing dipole moments. Thus for the β_1, which is associated with the benzyl moiety, the dipole is expected to be much smaller than for the β_2 mode which is of the cationic side chain. The relaxation times of the β_1 mode are consistent with those of β relaxation in polystyrene.[60]

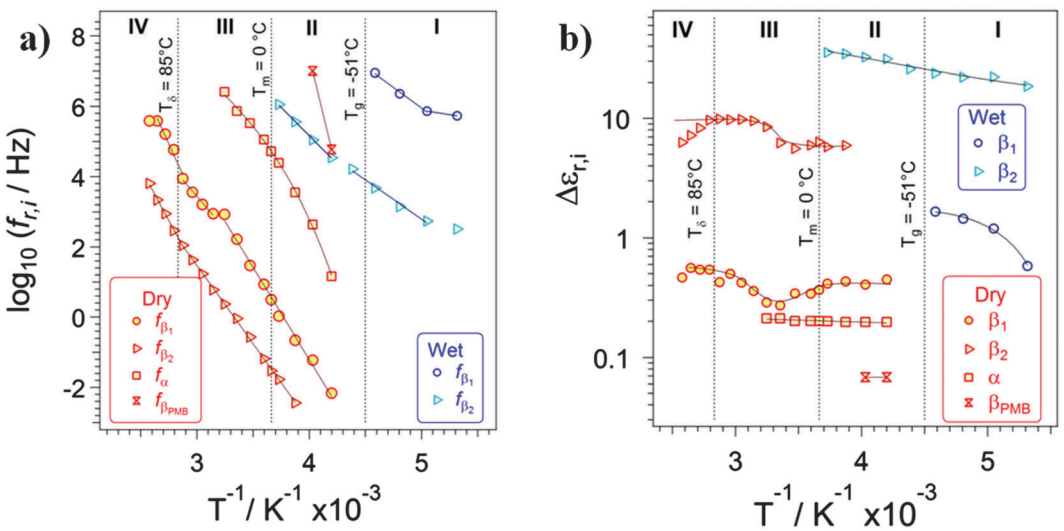

Fig. 8 Dependence on the reciprocal of temperature of relaxation frequencies (a), $f_{r,i}$, and dielectric strengths (b), $\Delta\varepsilon_{r,i}$, of both wet and dry [PVBTMA][Br]-*b*-PMB membranes in I, II, III and IV regions. $f_{r,i}$ *vs.* 1/*T* curves present Arrhenius-like behaviours. α – relaxation in the II and III region shows a VTF-behaviour.

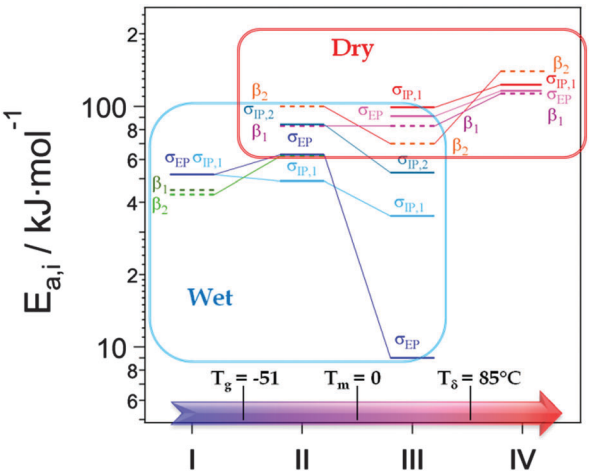

Fig. 9 Activation energies ($E_{a,i}$) of σ_i (σ_i = σ_{EP}, $\sigma_{IP,1}$ and $\sigma_{IP,2}$) and $f_{r,i}$ dielectric modes (i = β_1 and β_2) in regions I, II, III and IV. The compared values are determined by fitting the data of Fig. 7c and 8a with an Arrhenius-like equation.[63]

A comparison between the values of E_a associated with both the relaxation frequencies and the conductivities is given in Fig. 9 for each of the regions I, II, III and IV in increasing temperature. In all regions, the E_a values of the [PVBTMA][Br] β modes are very close to those of the σ_i conductivities in the dry membrane. The agreement between these values suggests that the mechanism of conduction, which takes place due to the exchange processes of anions between interaction sites in the hydrophilic A domains: (a) is decoupled from the motion of the main backbone polymer chains (segmental motion); and (b) is strongly influenced by the motion of the [PVBTMA$^+$][Br$^-$] side groups. In the wet membrane, the E_a values associated with the β_1 and β_2 are similar to those found for the wet conductivities (Fig. 9) below 0 °C (regions I and II). In this temperature regime, the dynamics of the water molecules is significantly inhibited, so the dynamics of the [PVBTMA$^+$][Br$^-$] side groups provide a significant contribution to the overall mechanism of conduction. In regions III and IV (above 0 °C and below T_δ) the dynamics of the side groups: (a) are decoupled from the charge transfer phenomena responsible for the conductivity pathway σ_{EP} (the E_a of σ_{EP} is one order of magnitude lower than that of β_1 and β_2 see Fig. 9); (b) are significantly correlated with the long range charge migration processes involved in the interdomain $\sigma_{IP,1}$ and $\sigma_{IP,2}$ conductivity pathways (the E_a values of β_1 and β_2 are of the same order of magnitude of $\sigma_{IP,1}$ and $\sigma_{IP,2}$). In the dry membrane under the same conditions, both σ_{EP} and $\sigma_{IP,1}$ are correlated with the β_1 and β_2 relaxations.

Taken all together, the results described above suggest that at $T > 0$ °C the overall conductivity (σ_T) of the membrane occurs as follows. In wet materials, σ_T is the result of the superposition of two conductivity pathways, $\sigma_T = \sigma_{EP} + \sigma_{IP,1}$. σ_{EP} is associated with the percolation migration pathway which exists when elementary Br$^-$ exchange events occur between different water clusters which are embedded in the hydrophobic A domains.

In this case the small water clusters act as macro-solvated anions ([H_2O]$_n$·Br$^-$) delocalizing Br$^-$ and facilitating its long range migration (no correlation with the β_1 and β_2 relaxations is expected). $\sigma_{IP,1}$ is attributed to a second percolation pathway that is formed when water solvated ion pairs in polar side chains, which have the dipole moment ip-μ exchange the anions (this percolation pathway has E_a similar to the β_2 relaxation mode). In the dry membrane where $\sigma_{EP} \approx \sigma_{IP,1}$, the long range charge migration percolation pathway occurs owing to the exchange of anions between polar side chains. In this case β_1 and β_2 relaxations play a crucial role in modulating both the σ_{EP} and $\sigma_{IP,1}$ percolation pathways, which consist of two physically different long range charge migration mechanisms characterized by two slightly different relaxation times.

Further insights into the role played by the local dynamics of ip-μ in the previously described conductivity pathways is obtained by correlating the diffusion coefficient of σ_{EP} (D_{EP}) and $\sigma_{IP,1}$ ($D_{IP,1}$) with the frequency of the β_2 relaxation mode for both the wet and dry membranes (Fig. 10). D_{EP} and $D_{IP,1}$ are determined as reported elsewhere[65] by using the following Nerst–Einstein equation (eqn (2)).

$$D_i = \frac{\sigma_i \cdot R \cdot T}{n_{Br} \cdot F^2} \quad (2)$$

where $n_{Br} = \varphi \cdot d$, $d = \left[m_{pol} + \sum_{i=1}^{n} m_i\right] \cdot \left[\frac{m_{pol}}{\rho_{pol}} + \sum_{i=1}^{n} \frac{m_i}{\rho_i}\right]^{-1}$, R is the gas constant, T is the absolute temperature, σ_i are the σ_{EP} or $\sigma_{IP,1}$ conductivity values, F is the Faraday constant, n_{Br} is the concentration of Br$^-$ anions, φ is the total anion exchange capacity, m_{pol} is the mass of the main polymer block (in this case that of the B block), m_i is the mass of the other i-th blocks, ρ_{pol} and ρ_i are the values of the density of the main and the i-th block polymer, respectively. The d values are obtained using the parameters reported elsewhere:[48] ρ[PVBTMA][Br] = 1.325 g cm^{-1}; ρ_{P4MS} = 1.04 g cm^{-1} and ρ_{PMB} = 0.9 g cm^{-1}.

For both the dry and wet membranes, the dependence of D_{EP} and $D_{IP,1}$ on the relaxation rate of the β_2 mode shows two distinct linear correlations (Fig. 10) which are satisfactorily fitted ($\chi^2 \sim 0.9$, see Fig. 10) by the Einstein–Smoluchowski equation:

$$D_i = \frac{\langle r_0 \rangle^2}{6\tau} = \frac{\pi \cdot \langle r_0 \rangle^2}{3} \cdot f_{\beta_2} = D_{0,i} f_{\beta_2} \quad (3)$$

where $D_{0,i} = \pi \cdot \langle r_0 \rangle^{2/3}$, τ the average time for the relaxation of ip-μ, and $\langle r_0 \rangle$ is the mean anion migration distance occurring at the T_g of the membrane or at a β_2 frequency (f_{β_2}) of 1 Hz. The behaviour of D confirms the results described above, and indicates that in the hydrophilic A domains the local fluctuations of the ip-μ's play a crucial role in the modulation of the long range Br$^-$ migration processes.

Furthermore, the goodness of fit of D_i *vs.* f_{β_2} (Einstein–Smoluchowski linear behaviour, Fig. 10) supports the previous hypothesis that in both dry and wet membranes the overall conductivity is the superposition of two types of percolating conductivity pathways in both the dry and wet membranes.

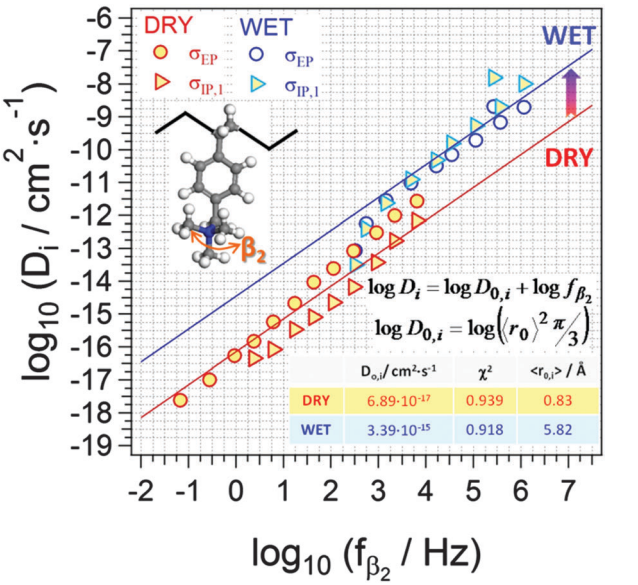

Fig. 10 Correlation of D_{σ_i} ($\sigma_i = \sigma_{EP}$ and $\sigma_{IP,1}$) with the f_{β_2} relaxation mode for dry and wet [PVBTMA][Br]-*b*-PMB membranes. D_{σ_i} values are evaluated as described in the text. Full lines show the Einstein–Smoluchowski-like fits obtained using the eqn (3). Parameters $D^0_{\sigma_i}$, $\langle r_0\rangle$ and χ^2 are reported. χ^2 is the correlation coefficient.

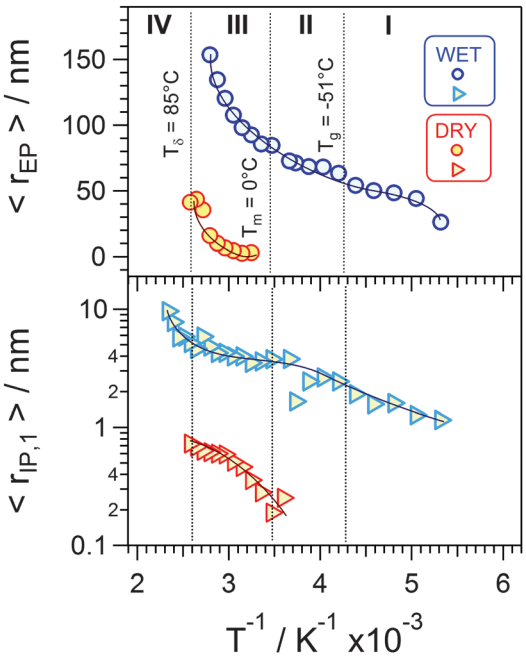

Fig. 11 Dependence of the average Br^- migration distance, $\langle r_i\rangle$, (i = EP and IP,1) on f_{β_2} the relaxation mode for dry and wet [PVBTMA][Br]-*b*-PMB membranes. $\langle r_i\rangle$ values are evaluated as described in the text.

These pathways are formed when ions are exchanged between fluctuating neighboring: (a) interaction sites of side chains for dry σ_{EP} and $\sigma_{IP,1}$ and wet $\sigma_{IP,1}$; (b) water clusters for σ_{EP}.

Therefore, in the dry membrane, the value of the mean migration distance at T_g (where the configurational entropy is minimized) $\langle r_0\rangle$ = 0.82 Å, which corresponds to the average separation distance between van der Waals radius of cations and anions in polar side chains of the A domains (as confirmed by DFT calculations), demonstrates that bellow T_g no Br^- exchange events between side groups are expected. In the wet membrane, the value of $\langle r_0\rangle$ = 5.82 Å indicates that the anion is solvated and that the exchange of the $[Br\cdot(H_2O)_n]$ complexes between –TMA^+ cationic side groups, which are separated by an average distance of *ca.* 7.3 Å, is highly probable.

Fig. 10 shows that in the wet material the D_i *vs.* f_{β_2} behavior is shifted to higher D_i values by about two orders of magnitude in comparison to the dry membrane. This indicates that water molecules facilitate the migration of the anion due to improved coupling phenomena between the ip-μ dynamics and the anion exchange processes. This is possible if we assume that in the hydrophilic A domains water coordinates preferentially to the anion forming $[Br\cdot(H_2O)_n]^-$ clusters, which are large and mobile anions strongly interacting with the polar side chains. These anionic species efficiently plasticize the hydrophilic A domains.

Further insights into the conductivity mechanisms are obtained by analyzing the dependence on temperature of the average anion migration distance of both the electrode polarization and the inter domain polarization phenomena, $\langle r_{EP}\rangle$ and $\langle r_{IP,1}\rangle$ respectively (Fig. 11). $\langle r_{EP}\rangle$ and $\langle r_{IP,1}\rangle$ are determined as reported elsewhere[47,66] by using the Einstein–Smoluchowski equation (eqn 4):

$$\langle r_i\rangle = \sqrt{6 \cdot D_i \cdot \tau_j}; \quad (4)$$

where the D_i values are reported in Fig. 10 and, τ_j, are the relaxation times of the EP and IP polarization events determined by the fitting of the data to eqn 1.

As the temperature rises, $\langle r_{EP}\rangle$ and $\langle r_{IP,1}\rangle$ increase for both the dry and wet membranes (Fig. 11) confirming that the charge migration process is a thermally stimulated event. In region III (temperature range 0 to 80 °C) $\langle r_{EP}\rangle$ increases exponentially from 70 to *ca.* 130 nm and from 0.5 to *ca.* 50 nm for the wet and dry membranes respectively (Fig. 11).

These observations are perfectly consistent with the SAXS results described above, for which the wet and dry membrane at 60 °C present an inter-lamellar *d*-spacing of 97 and 45 nm, respectively. This observation suggests that along the σ_{EP} conductivity pathway, the charge migration mechanism consists of Br^- exchanges between neighboring water clusters impregnating specific volumes of the A domains. In the [PVBTMA][Br]-*b*-PMB membrane, the volume of the membrane where the anion can be considered delocalized on the time scale of the exchange processes responsible for the long range charge migration processes typical of conductivity is defined as the delocalization body (DB). The DB concept was recently proposed for proton conducting membranes.[46] These DBs in the membranes at low hydration levels or at low temperatures are smaller than the total volume of the A domains. As the membrane hydration level rises the DB increases wetting the entire A domain in the fully hydrated or swelled membranes. In the latter case the average

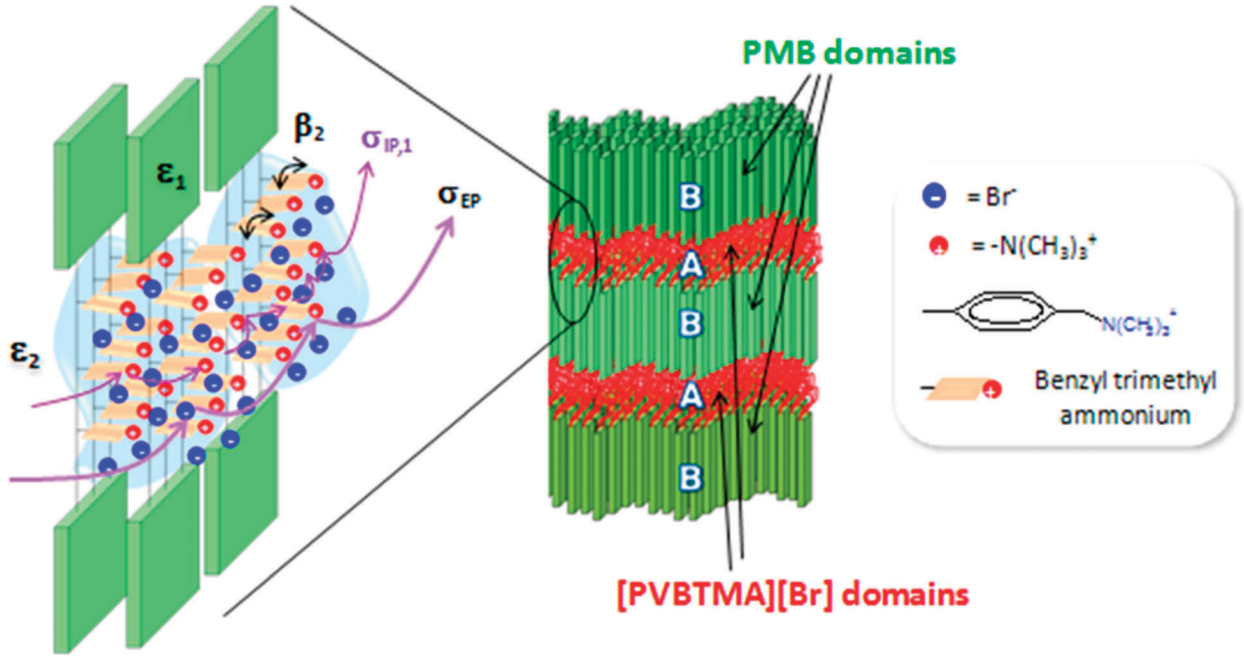

Scheme 4 Proposed conduction mechanism for [PVBTMA][Br]-*b*-PMB membranes. σ_{EP} and $\sigma_{IP,1}$ are the percolation conductivity pathways discussed in the text. ε_1 and ε_2 are the permittivity of B and A blocks, respectively.

migration distance coincides with the inter-A domain separation distance. In this last situation, the exchange of anions between DBs is identified with an inter-A domain migration event of Br^-. In general the σ_{EP} mechanism is significantly modulated by the local dipole fluctuations of $-TMA^+$ side groups. An exception is the fully hydrated state of the membrane in III (at $T > 0$ °C), where decoupling of the dynamics of polar side chains from the charge migration events is revealed. In region III and IV up to the T_δ transition, $\langle r_{IP,1} \rangle$ increases from 3 to *ca.* 5 nm and from 0.1 to 0.6 nm, respectively, for the wet and dry membrane (Fig. 11). This indicates that for $\sigma_{IP,1}$: (a) in the wet membrane, there is a percolation pathway where the anion is exchanged between $[Br\cdot(H_2O)_n]^-$ clusters neutralizing the $-TMA^+$ side chains; and (b) in the dry membrane, if we consider that the structural average distance between the polar side chains is *ca.* 0.7 nm (as determined by DFT calculations), there is a percolation pathway formed by simple anion exchange processes between neighbouring polar side chains.

The BES results merged with structural and thermo-mechanical information are useful to explain in a reasonable manner the mechanisms governing the overall conductivity mechanism in the dry and wet [PVBTMA][Br]-*b*-PMB membranes (Scheme 4). If we consider that $\sigma_{IP,2} \ll \sigma_{IP,1}$, the overall conductivity (σ_T) of both the dry and fully hydrated [PVBTMA][Br]-*b*-PMB membrane is the superposition of two concurring percolation pathways, $\sigma_T = \sigma_{EP} + \sigma_{IP,1}$, which are associated with two different physical phenomena.

$\sigma_{IP,1}$ is a percolation pathway where concerted exchange of anions between $-TMA^+$ cations (Scheme 4) takes place. In wet membranes Br^- is exchanged between $[Br\cdot(H_2O)_n]^-$ anionic water complexes neutralizing the $-TMA^+$ side chains. These phenomena are assisted by: (a) β_2 relaxation, *i.e.* the dynamics of ip-μ dipoles; and (b) the stability and structural features of the $[Br\cdot(H_2O)_n]^-$ anionic water complexes closely interacting with $-TMA^+$ cations for the membrane in the hydrated state.

σ_{EP} is a percolation pathway where Br^- is exchanged between the different DBs present in the bulk membranes (Scheme 4).

Conclusions

The structural features, thermomechanical properties, and the electrical response of a diblock [PVBTMA][Br]-*b*-PMB membrane (where A is the [PVBTMA][Br] hydrophilic domain and B is the PMB hydrophobic one) are studied by SAXS, HR-TG, MDSC, DMA, and BES techniques. SAXS results reveal a long range ordered lamellar morphology with a *d*-spacing that changes from 45 to 97 nm as the hydration of the membrane changes from the dry to the wet state at 60 °C. HR-TG, MDSC, and DMA studies show that the membrane is thermally stable up to *ca.* 140 °C. Two main thermal transitions are present: (a) a glass transition at $T_g = -51$ °C; and (b) a new unexpected disorder–order transition (T_δ) which decreases from *ca.* 115 to *ca.* 85 °C on going from the dry to the wet membrane.

T_δ is associated with a solid-state structural rearrangement which takes place in the A domain when strong electrostatic interchain interactions between ion-pair dipole moments (ip-μ's) occur. The phenomenon responsible for T_δ plays a crucial role in modulating the properties of membranes.

The analysis of the electric response of the membrane in terms of complex $\varepsilon^*(\omega)$, $\sigma^*(\omega)$ and $\tan\delta(\omega)$ is performed by BES studies. In the dry membrane, three polarization events (σ_{EP}, $\sigma_{IP,1}$ and $\sigma_{IP,2}$) and four molecular relaxations (α and β_{PMB}) modes for PMB blocks of B domains; β_1 and β_2 modes for the

relaxations of the benzyl and polar quaternary ammonium (ip-μ side chains, respectively, in hydrophilic A domains) are revealed. Furthermore, for the fully hydrated [PVBTMA][Br]-*b*-[PMB] membrane, evidence is seen for the following phenomena: (a) four conductivity regions (I, II, III and IV) delimited by the thermal transitions (*i.e.* T_g, T_m, and T_δ); (b) two polarization events at $T > 0$ °C (σ_{EP} and $\sigma_{IP,1}$), which dominate the electric response; and (c) two dielectric relaxations at $T < 0$ °C (β_1 and β_2), which are superimposed to the σ_{EP}, and $\sigma_{IP,1}$ polarizations. It is revealed that the overall conductivity of the [PVBTMA][Br]-*b*-[PMB] membrane is the superposition of two conductivity percolation pathways ($\sigma_T = \sigma_{EP} + \sigma_{IP,1}$) modulated by the dipole moment fluctuations of the polar side groups (β_2 mode) in the A domains. In detail, σ_{EP} and $\sigma_{IP,1}$ are two types of physically different percolating long range charge migration pathways. In $\sigma_{IP,1}$ the long range Br^- migration occurs owing to a concerted exchange of anions between $-TMA^+$ cations. These events are correlated with the structure of anion-H_2O coordination processes and with the dynamics of the β_2 mode. In the σ_{EP} percolation pathway the long range charge migration processes occur by Br^- exchanges between different delocalization bodies (DBs) present in the A domains. The results reported here are of crucial importance in order to understand the phenomena modulating the properties of alkaline membranes for electrochemical applications and provide an important diagnostic background to use for improving these materials.

Acknowledgements

This research was funded by grant W911NF-13-1-0400, entitled ''Interplay between relaxations and structure in anion-exchange membranes (AEMs) by broadband electrical spectroscopy (BES), thermomechanical and vibrational studies'' awarded by the U.S. Army Research Office (ARO) in the framework of the ARO sponsored MURI project ''An Integrated Multi-Scale Approach for Understanding Ion Transport in Complex Heterogeneous Organic Materials'' grant W911NF-10-1-0520. This research was funded equally by the Strategic Project of the University of Padova ''MAESTRA – From Materials for Membrane-Electrode Assemblies to Electric Energy Conversion and Storage Devices'' and also by Veneto Nanotech S.C.p.a. (Venice). This research used resources of the Advanced Photon Source, a U. S. Department of Energy (DOE) Office of Science User Facility operated for the DOE Office of Science by Argonne National Laboratory under Contract No. DE-AC02-06CH11357. G. G. acknowledges the financial support of the ''Helmholtz-Energie-Allianz-Stationäre elektrochemische Feststoff-Speicher und-Wandler'' (Förderkennzeichen: HA-E-0002).

References

1 J. R. Varcoe and R. C. T. Slade, *Fuel Cells*, 2005, **5**, 187–200.
2 J. R. Varcoe, P. Atanassov, D. R. Dekel, A. M. Herring, M. A. Hickner, P. A. Kohl, A. R. Kucernak, W. E. Mustain, K. Nijmeijer, K. Scott, T. Xu and L. Zhuang, *Energy Environ. Sci.*, 2014, **7**, 3135–3191.
3 *Membrane Science and Technology*, ed. S. Heiner, Elsevier, 2004, vol. 9.
4 V. Di Noto, T. A. Zawodzinski, A. M. Herring, G. A. Giffin, E. Negro and S. Lavina, *Int. J. Hydrogen Energy*, 2012, **37**, 6120–6131.
5 S. Marini, P. Salvi, P. Nelli, R. Pesenti, M. Villa, M. Berrettoni, G. Zangari and Y. Kiros, *Electrochim. Acta*, 2012, **82**, 384–391.
6 W. Wang, Q. Luo, B. Li, X. Wei, L. Li and Z. Yang, *Adv. Funct. Mater.*, 2013, **23**, 970–986.
7 B. E. Logan and M. Elimelech, *Nature*, 2012, **488**, 313–319.
8 J. X. Leong, W. R. W. Daud, M. Ghasemi, K. Ben Liew and M. Ismail, *Renewable Sustainable Energy Rev.*, 2013, **28**, 575–587.
9 W. Gellett, J. Schumacher, M. Kesmez, D. Le and S. D. Minteer, *J. Electrochem. Soc.*, 2010, **157**, B557–B562.
10 S.-W. C. Ryan O'Hayre, W. Colella, F. B. Prinz, *Fuel Cell Fundamentals*, 2006, pp. 26–30.
11 W. Vielstich, in *Handbook of fuel cells*, ed. W. Vielstich, A. Lamm and H. Gasteiger, Wiley, Chichester, 2003, vol. 1, pp. 26–30.
12 J. S. Spendelow and A. Wieckowski, *Phys. Chem. Chem. Phys.*, 2007, **9**, 2654–2675.
13 V. Di Noto, S. Lavina, G. A. Giffin, E. Negro and B. Scrosati, *Electrochim. Acta*, 2011, **57**, 4–13.
14 *CRC Handbook of Chemistry and Physics*, CRC press, 2007.
15 M. G. Marino, J. P. Melchior, A. Wohlfarth and K. D. Kreuer, *J. Membr. Sci.*, 2014, **464**, 61–71.
16 G. Merle, M. Wessling and K. Nijmeijer, *J. Membr. Sci.*, 2011, **377**, 1–35.
17 G. G. Wang, Y. M. Weng, D. Chu, R. R. Chen and D. Xie, *J. Membr. Sci.*, 2009, **332**, 63–68.
18 J. L. Yan and M. A. Hickner, *Macromolecules*, 2010, **43**, 2349–2356.
19 C. G. Arges, M. S. Jung, G. Johnson, J. Parrondo and V. Ramani, *ECS Trans.*, 2011, **41**, 1795–1816.
20 X. Li, Q. Liu, Y. Yu and Y. Meng, *J. Mater. Chem. A*, 2013, **1**, 4324–4335.
21 Z. Liu, X. Li, K. Shen, P. Feng, Y. Zhang, X. Xu, W. Hu, Z. Jiang, B. Liu and M. D. Guiver, *J. Mater. Chem. A*, 2013, **1**, 6481–6488.
22 C. H. Fujimoto, M. A. Hickner, C. J. Cornelius and D. A. Loy, *Macromolecules*, 2005, **38**, 5010–5016.
23 M. R. Hibbs, C. H. Fujimoto and C. J. Cornelius, *Macromolecules*, 2009, **42**, 8316–8321.
24 T. W. Xu and W. H. Yang, *J. Membr. Sci.*, 2001, **190**, 159–166.
25 L. Wu, T. W. Xu, D. Wu and X. Zheng, *J. Membr. Sci.*, 2008, **310**, 577–585.
26 L. Wu and T. W. Xu, *J. Membr. Sci.*, 2008, **322**, 286–292.
27 Y. Yang and D. M. Knauss, *Macromolecules*, 2015, **48**, 4471–4480.
28 R. Vinodh, A. Ilakkiya, S. Elamathi and D. Sangeetha, *Mater. Sci. Eng., B*, 2010, **167**, 43–50.

29 Q. H. Zeng, Q. L. Liu, I. Broadwell, A. M. Zhu, Y. Xiong and X. P. Tu, *J. Membr. Sci.*, 2010, **349**, 237–243.
30 J. L. Wang, R. H. He and Q. T. Che, *J. Colloid Interface Sci.*, 2011, **361**, 219–225.
31 T.-H. Tsai, A. M. Maes, M. A. Vandiver, C. Versek, S. Seifert, M. Tuominen, M. W. Liberatore, A. M. Herring and E. B. Coughlin, *J. Polym. Sci., Part B: Polym. Phys.*, 2013, **51**, 1751–1760.
32 M. A. Vandiver, B. R. Caire, Z. Poskin, Y. Li, S. Seifert, D. M. Knauss, A. M. Herring and M. W. Liberatore, *J. Appl. Polym. Sci.*, 2015, **132**, 41596, DOI: 10.1002/app.41596.
33 J. R. Varcoe, R. C. T. Slade, E. L. H. Yee, S. D. Poynton, D. J. Driscoll and D. C. Apperley, *Chem. Mater.*, 2007, **19**, 2686–2693.
34 K. J. T. Noonan, K. M. Hugar, H. A. Kostalik, E. B. Lobkovsky, H. D. Abruna and G. W. Coates, *J. Am. Chem. Soc.*, 2012, **134**, 18161–18164.
35 M. Zhang, H. K. Kim, E. Chalkova, F. Mark, S. N. Lvov and T. C. M. Chung, *Macromolecules*, 2011, **44**, 5937–5946.
36 T.-H. Tsai, S. P. Ertem, A. M. Maes, S. Seifert, A. M. Herring and E. B. Coughlin, *Macromolecules*, 2015, **48**, 655–662.
37 G. G. Wang, Y. M. Weng, D. Chu, D. Xie and R. R. Chen, *J. Membr. Sci.*, 2009, **326**, 4–8.
38 G. H. Wang, Y. M. Weng, J. Zhao, D. Chu, D. Xie and R. R. Chen, *Polym. Adv. Technol.*, 2010, **21**, 554–560.
39 T. P. Pandey, A. M. Maes, H. N. Sarode, B. D. Peters, S. Lavina, K. Vezzu, Y. Yang, S. D. Poynton, J. R. Varcoe, S. Seifert, M. W. Liberatore, V. Di Noto and A. M. Herring, *Phys. Chem. Chem. Phys.*, 2015, **17**, 4367–4378.
40 G. Couture, A. Alaaeddine, F. Boschet and B. Ameduri, *Prog. Polym. Sci.*, 2011, **36**, 1521–1557.
41 M. L. Disabb-Miller, Z. D. Johnson and M. A. Hickner, *Macromolecules*, 2013, **46**, 949–956.
42 M. R. Hibbs, M. A. Hickner, T. M. Alam, S. K. McIntyre, C. H. Fujimoto and C. J. Cornelius, *Chem. Mater.*, 2008, **20**, 2566–2573.
43 M. G. Marino and K. D. Kreuer, *ChemSusChem*, 2015, **8**, 513–523.
44 G. A. Giffin, S. Lavina, G. Pace and V. Di Noto, *J. Phys. Chem. C*, 2012, **116**, 23965–23973.
45 G. A. Giffin, G. M. Haugen, S. J. Hamrock and V. Di Noto, *J. Am. Chem. Soc.*, 2013, **135**, 822–834.
46 V. Di Noto, M. Piga, G. A. Giffin, K. Vezzu and T. A. Zawodzinski, *J. Am. Chem. Soc.*, 2012, **134**, 19099–19107.
47 V. Di Noto, N. Boaretto, E. Negro, P. E. Stallworth, S. Lavina, G. A. Giffin and S. G. Greenbaum, *Int. J. Hydrogen Energy*, 2012, **37**, 6215–6227.
48 T.-H. Tsai, PhD thesis, University of Massachusetts, Amherst, 2013.
49 M. Vittadello, E. Negro, S. Lavina, G. Pace, A. Safari and V. Di Noto, *J. Phys. Chem. B*, 2008, **112**, 16590–16600.
50 Y. Liu, J. L. Horan, G. J. Schlichting, B. R. Caire, M. W. Liberatore, S. J. Hamrock, G. M. Haugen, M. A. Yandrasits, S. Seifert and A. M. Herring, *Macromolecules*, 2012, **45**, 7495–7503.
51 B. Delley, *J. Chem. Phys.*, 1990, **92**, 508–517.
52 B. Delley, *J. Chem. Phys.*, 2000, **113**, 7756–7764.
53 D. C. Herbst, T. A. Witten, T.-H. Tsai, E. B. Coughlin, A. M. Maes and A. M. Herring, *J. Chem. Phys.*, 2015, **142**, 114906.
54 M. J. Park and N. P. Balsara, *Macromolecules*, 2008, **41**, 3678–3687.
55 I. Petrariu, C. Luca, I. G. Poinescu and M. Dima, *Rev. Roum. Chim.*, 1973, **18**, 493.
56 W. Hu, H. Hagihara and T. Miyoshi, *Macromolecules*, 2007, **40**, 1763–1766.
57 R. Katritzky, S. Sild, V. Lobanov and M. Karelson, *J. Chem. Inf. Comput. Sci.*, 1998, **38**, 300–304.
58 V. Di Noto, M. Piga, S. Lavina, E. Negro, K. Yoshida, R. Ito and T. Furukawa, *Electrochim. Acta*, 2010, **55**, 1431–1444.
59 V. Di Noto, G. A. Giffin, K. Vezzù, M. Piga and S. Lavina, in *Solid State Proton Conductors: Properties and Applications in Fuel Cells*, ed. P. Knauth and M. L. Di Vona, John Wiley and Sons, 2012, pp. 109–183, DOI: 10.1002/9781119962502.ch5.
60 N. G. McCrum, in *Anelastic and Dielectric Effects in Polymeric Solids*, ed. N. G. McCrum, B. E. Read and G. Williams, Dover Publications, New York, 1967.
61 V. Di Noto, M. Piga, G. Pace, E. Negro and S. Lavina, *ECS Trans.*, 2008, **16**, 1183–1193.
62 V. Di Noto, M. Piga, L. Piga, S. Polizzi and E. Negro, *J. Power Sources*, 2008, **178**, 561–574.
63 V. Di Noto, *J. Phys. Chem. B*, 2002, **106**, 11139–11154.
64 C. J. F. B. P. Bordewijk, *Theory of Electric Polarization, Vol. 2: Dielectrics in Time-Dependent Fields*, 2nd edn, 1980.
65 V. Di Noto, M. Vittadello, K. Yoshida, S. Lavina, E. Negro and T. Furukawa, *Electrochim. Acta*, 2011, **57**, 192–200.
66 V. Di Noto, M. Vittadello, S. G. Greenbaum, S. Suarez, K. Kano and T. Furukawa, *J. Phys. Chem. B*, 2004, **108**, 18832–18844.